Weak link properties of $YBa_2Cu_3O_7$ nanostructures

M.V. Pedyash, D.H.A. Blank and H. Rogalla

Low Temperature Division, Department of Applied Physics, University of Twente, P.O.Box 217, 7500 AE Enschede, The Netherlands.

ABSTRACT

$YBa_2Cu_3O_7$ bridges with widths ranging from 50nm to 3μm were made using Electron Beam Lithography and Focused Ion Beam milling. The current voltage characteristics of the nanobridges show, under microwave irradiation, pronounced Shapiro steps up to the transition temperature. SQUIDs, using these nanobridges, have been made and flux to voltage modulation up to 85K was observed, with a maximum modulation depth of 8 μV at 77K. An unusual temperature dependence of the modulation is observed, which can be explained by assuming an exponential spatial distribution of the superconducting properties near the edge of a superconductor.

Keywords: High Temperature Superconductivity, nanobridges, SQUIDs, surface vortex pinning

1. INTRODUCTION

Superconducting nanobridges are very intrigued, due to the fact that these relative simple structures show Josephson effect[1]. In theory, only nanobridges that have dimensions comparable with the coherence length ξ are expected to show true Josephson behaviour [2,3]. In practice, it is found that bridges with dimensions comparable with the effective magnetic field penetration depth λ_{eff} exhibit Josephson-like effects, like Shapiro steps under microwave irradiation [4]. The concept of the coherent motion of flux quanta has become a standard for nanobridges description, and explains a wide variety of effects [5]. However, the periodic supercurrent-phase relation, which is the principle of SQUID operation, does not result evidently from this model.

In this article we present the characteristics of nanobridge junctions together with nanobridge SQUIDs, made either by electron beam lithography or Focused Ion Beam milling. Besides IV-characteristics, the response of the nanobridges to microwave irradiation has been investigated. We explain the Josephson nature of these devices by considering degradation of the bridge area during structuring, which leads to a transition from a SNS to SS'S type junction with decreasing temperature. Furthermore, we derive the shape of the vortex surface barrier assuming the suppression of superconducting properties at the superconductor edge. Following this approach, current voltage characteristics of nanobridges are calculated and compared with the experimental data. Finally, the dependence of the critical supercurrent I_c on the nanobridge width is discussed.

2. NANOBRIDGE AND SQUID PREPARATION

Nanobridges were prepared by, both, electron beam lithography (EBL) and direct Focused Ion Beam milling (FIB). With the former technique, dimensions down to 50nm could be obtained [6]. With the latter technique trenches are etched in thin YBCO films (thickness ≤ 100nm), using a 25 kV Ga^+ beam with a diameter of 50 nm (FWHM) [7]. The depth profiles and dimensions of these nanobridges were determined using Scanning Force Microscopy (SFM). The length of the bridges (150nm) is defined by the spot size of the FIB system. The depth of the milled lines has been taken 140 % of the film thickness (which was in most cases approximately 100nm). The edges of the nanobridges have generally a Gaussian shape, due to the shape of the beam profile. Consequently, the width of the bridges is approximately 100nm less than designed before FIB milling. The electrical isolation of the milled trenches was determined by an "open bridge". The resistance of this structure was > 40 MΩ, so we conclude that the electrodes of the nanobridges were electrically isolated. All $YBa_2Cu_3O_7$ layers were prepared by the pulsed laser deposition technique [8]. The transition temperature T_c of unstructured films is (90±1) K.

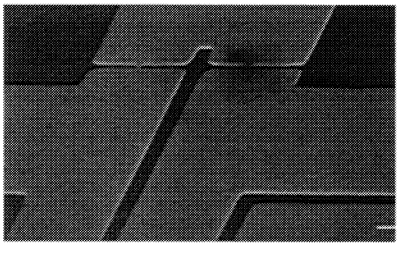

Fig.1(a) Micrograph of nano-SQUID.

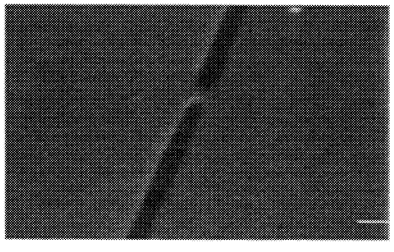

Fig.1(b) Micrograph of one of the nanobridges.

0-8194-2071-9/96/$6.00

SQUIDs, using these nanobridges, have been realized. Here, an inductively shunted (directly coupled) single layer dc-SQUID geometry was chosen. Fig. 1(a) shows a micrograph of the SQUID fragment and in fig 1(b) one of the nanobridge junctions can be seen. In this example, the nanobridges are 150nm long and 250nm wide, the slit is 0.6μm wide and 55μm long and the SQUID pick-up loop is 8mm squared.

3. EXPERIMENTAL

3.1 Nanobridges

In Fig.2 the current-voltage characteristics are given for different bridge widths. The critical temperature of the nanobridges with widths wider than 250nm did not change significantly from the unstructured films. Below 250nm, the superconducting transition curves R(T) show the presence of a "foot" that grows rapidly with decreasing width, see Fig.2(b). The critical current I_c is a linear function of the nanobridge width w for 50 nm < w < 350 nm. The critical current density J_c is up to $3 \cdot 10^6$ A/cm^2 at 77 K and follows $J_c \propto (1-T/T_c)^{1.6\pm0.1}$ in a wide range of temperatures from T_c down to at least $T_c/2$.

The Josephson-like behaviour of the nanobridges has been verified with microwave irradiation. Shapiro steps can be clearly seen up to 1K below Tc.

3.2 SQUIDs

The current-voltage characteristics of SQUIDs at zero external magnetic field are similar to those of single nanobridges. With our SQUIDs made from these nanobridges, voltage-flux modulation was observed for w< 300 nm. The maximum detected peak to peak voltage modulation U_{mod} is 8 μV at 77K for the device based on 250 nm bridges (Fig.3) and 45 μV at 4.2 K (100 nm bridges). The SQUID effective sensing area $A_{eff}=\Phi_0/B_0$ is calculated, using the period of the voltage-flux modulation B_0. Here, we found an A_{eff} of 0.07 mm^2 at 4.2 K, which increases at higher temperatures (Fig. 4). Taking into account that in an inductively shunted SQUID the pick-up loop is much larger than the SQUID loop, flux in the SQUID can be written as: $\Phi=B \cdot A_p L_{sq}/L_p$, where A_p is the pick-up loop area, L_p is the pick-up loop inductance and L_{sq} is the inductance of the SQUID loop. L_{sq} is estimated to be 20 pH at T=4.2 K. We assume that A_p and L_p depend on the geometry of the device and not on temperature. Both, kinetic and geometrical terms of the SQUID inductance are functions of the magnetic field penetration depth λ(T). Taking $\lambda(T)=\lambda_0/(1-(T/T_c)^2)^{1/2}$, where λ_0 is the penetration depth at zero temperature, the experimental data can be fitted with λ_0=180 nm (the drawn line in Fig.4).

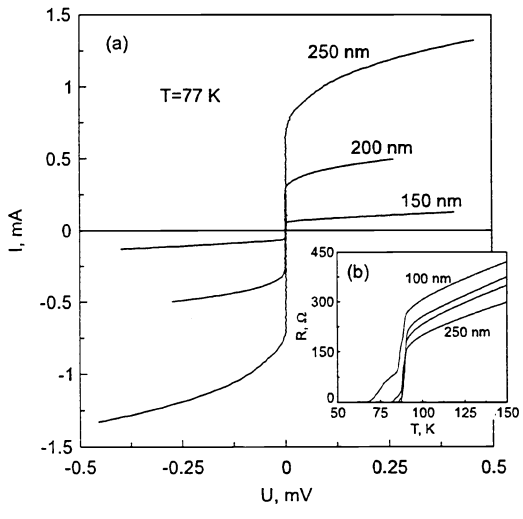

Fig.2 The I(V) (a) and R(T) (b) characteristics of nanobridges with different width.

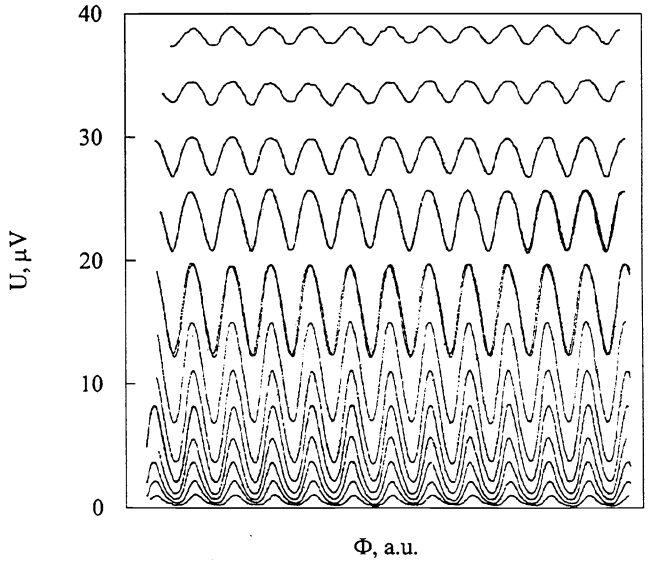

Fig.3 A typical voltage-flux modulation of a nanobridge SQUID for different bias voltages (w=250nm, T=77K).

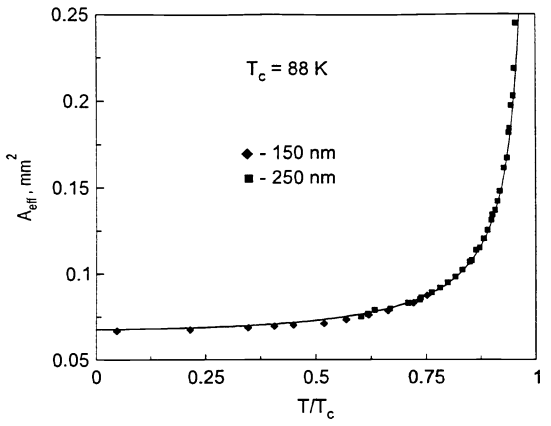

Fig.4 Temperature dependence of the effective sensing area A_{eff} of two different SQUIDs. The solid line is the model fit.

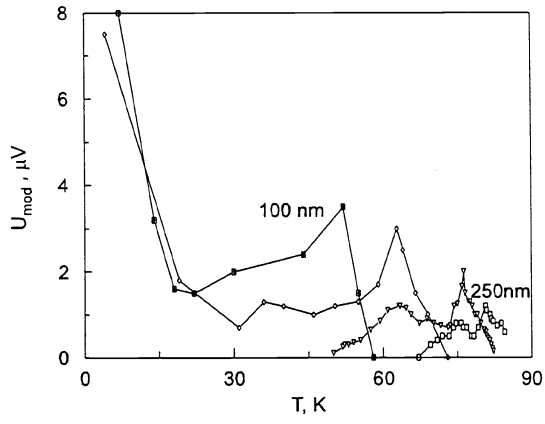

Fig.5 Experimental values of $U_{mod}(T)$ for SQUIDs with nanobridges of different width (w=100, 150, 200, 250nm).

The temperature dependence of the voltage modulation $U_{mod}(T)$ of the nanobridge SQUID differs from conventional weak link SQUIDs, as described by the RSJ model. For wider bridges (200-300nm), the amplitude of the modulation increases fast with decreasing temperature and reaches quite a narrow maximum at $T \approx 0.9T_c$. With further decrease of temperature the amplitude of modulation decreases and vanishes, remaining zero at lower temperature. Using very narrow bridges (<150nm), where T_c is suppressed significantly, the voltage modulation shows again a maximum at higher temperature, a decrease of the voltage modulation in intermediate temperature range, and, in contrast to the former experiments, an abrupt increase at low temperatures (typically below 20 K). In Fig.5, these results are plotted. Each data point is the maximum modulation voltages obtained at corresponding temperature. This behaviour can not be explained by an increase of the SQUID screening parameter $\beta_L = 2I_cL_{sq}/\Phi_0$ due to the increase of I_c with decreasing temperature. The increase of β_L leads to a saturation of the modulation amplitude and not to a suppression.

4. DISCUSSION

4.1 Weak link behaviour

The superconducting properties of $YBa_2Cu_3O_7$ degrade in the vicinity of a trench patterned by either EBL or FIB. The origin of this degradation is due to, e.g., irradiation by high energy ions [9] or thermal and chemical treatments, which leads to oxygen diffusion [10]. This degraded region will have a significant length of several nm, along which the superconducting properties change. We assume that the spatial distribution of T_c in a region close to the trench follows the formula:

$$T_c(x) = T_{cb}(1 - e^{-X/X_o}), \quad (1)$$

where T_{cb} is the critical temperature of bulk, x is the distance from the trench and x_0 is the characteristic length of T_c variation. Applying this formula to our nanobridges, (i.e. two trenches at distance w=2x), a decrease of T_c of the nanobridge with decreasing w is expected. This is confirmed by the experimental results (see Fig.2(b)), taking x_0 in the order of 30-50 nm.

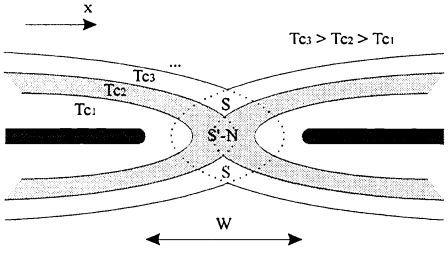

Fig.6 Schematic critical temperature distribution inside the nanobridge area.

Applying this assumption to our nanobridges, they can be considered as an SNS type junction in the temperature range of $T_{c2} < T < T_{c3}$, and as an all-superconductor below T_{c2}, where T_{c2} is the critical temperature of the middle of the bridge, and T_{c3} the critical temperature of the layer next to it. In Fig.6 a schematic illustration is given. Both, T_{c2} and T_{c3} are functions of w. Such representation can be described by the "two fluid" model, where the Josephson component of the supercurrent I_j is gradually substituted by a "strong" (i.e. non-periodic with the phase difference $\Delta\varphi$) term with decreasing temperature. Assuming T_c of the bridge according to (1), the temperature dependence I_j, for

long SS'S junctions, can be calculated according to Likharev and Kupriyanov [3,11]:

$$I_j = \frac{const \cdot I_C(T)}{(1+\sqrt{1+A^2/2})^2} \cdot \exp(-L/\xi) \ . \qquad (2)$$

Here, $A^2 = (T_{cs} - T)/|T_c - T|$, where T_{cs} is the critical temperature of the junction electrodes and T_c the one of the junction area itself. L is the length of the junction. We substituted in the model T_{cs} by T_{c3} and T_c by T_{c2}, where, both, T_{c2} and T_{c3} are functions of the bridge width w according to (1).

In Fig. 7(a) the results of these calculation are given. The SQUID voltage modulation is proportional to the critical current I_c (assumed to be the Josephson current) and can be written as [12]:

$$U_{\mathrm{mod}} = \frac{7}{\pi^2} \cdot \frac{I_c R_n}{1+\beta_L} \left(1 - 3.57 \frac{\sqrt{k_b T \cdot L_{sq}}}{\Phi_0} \right) \ . \qquad (3)$$

This expression explains the disappearing of the SQUID modulation at lower temperatures due to declination of the Josephson term I_j of the full supercurrent of the nanobridge. By assuming a T_c distribution along the bridge according to (1), the temperature range, where the modulation is observed, can be calculated and agrees with the experiment for the bridges of all widths.

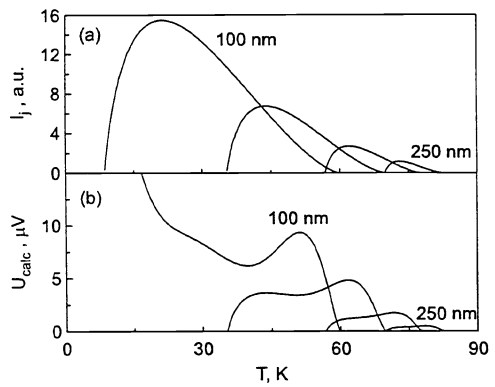

Fig.7 Calculated Josephson current component I_j (a) and the amplitude of the voltage-flux modulation U_{calc} (b) for SQUIDs with bridges of different width.

In contrast to conventional Josephson weak link devices, which can be described by the RSJ model, the nanobridge SQUID is a typical "flux-flow" device with corresponding I-V characteristics [13]. Instead of a single and well defined RSJ like resistance parameter R_n, the nanobridge SQUID is characterized by the dynamic resistance R_{dyn}, which is determined by effects of vortex flow in the bridge and can depend on temperature in a rather complicated way. R_{dyn} was measured experimentally and increases strongly in, both, low and high temperature regions. Subsequently, the SQUID voltage modulation U_{calc} was calculated as a function of temperature for the bridges of different width, using equation (3), taking the experimental values of R_{dyn} and the calculated $I_j(T)$, see Fig. 7(b). A qualitative agreement between the experimental data and the calculated U_{calc} have been obtained for all temperatures and bridge widths (compare Fig.5 and Fig.7(b)).

A more realistic assumption would be that even at high temperatures only a small fraction of the total supercurrent in the bridge is of Josephson origin. This is in agreement with the high obtained values of J_c at 77 K. Furthermore, this would explain the absence of any serious suppression of I_c by a weak magnetic field. The above assumption means that vortices in the nanobridges are not only of the Abrikosov type, but can gain properties of Josephson fluxons, like increase of the vortex size and gradual disappearance of the normal vortex core with decreasing w [3]. The proposed $T_c(x)$ distribution near the bridge edge leads to a more complicated shape of the edge barrier for a vortex to enter the bridge.

4.2 Vortex edge pinning.

In earlier works dedicated to vortex motion in nanobridges it was shown that, even in case of zero external magnetic field, the surface barrier for a vortex to penetrate to the superconductor significantly exceeded the Gibbs free energy of a vortex [5]. This means that, even at absence of bulk pinning in nanobridges, the critical supercurrent is determined by pinning of vortices by the edge of a structure and not by the first critical magnetic field H_{c1}. The origin of this surface barrier, or "geometrical barrier", assumed to be the interaction of a vortex with the superconductor surface, i.e., with the vacuum - ideal superconductor

interface. As it has been discussed above, this is not the case for high temperature superconductors. Near the nanobridge edge λ can, in an analogy to T_c, be approximated by:

$$\lambda(x) = \frac{\lambda_0}{1 - e^{-x/x_0}}, \qquad (4)$$

with λ_0 is the London magnetic field penetration depth. We substitute this expression for λ into the Poisson equation for the magnetic of a vortex field $\mathbf{h}(\mathbf{r})$ [14]:

$$\nabla^2 \mathbf{h} - \frac{\mathbf{h}}{\lambda^2(x)} = \frac{\Phi_0}{\lambda^2(x)} \mathbf{z}\delta(\mathbf{r}) . \qquad (5)$$

Here, Φ_0 is the magnetic flux quantum, $\mathbf{z}$ is a unit vector along the vortex and $\delta(\mathbf{r})$ is a two-dimensional delta function at the location of the vortex core. This equation was solved numerically. Knowing the magnetic field distribution of a vortex near the sample edge, the interaction of the vortex with it's image, i.e., the surface pinning potential was calculated. In Fig. 8 the calculated force acting on the vortex due to an interaction with the surface is presented. The profile of the barrier depends on x_0 and, in the extreme case of x_0=0, transforms to the known Bean-Livingston surface barrier. For the discussed barrier, the choice of the nucleation position affects much less the overall energy barrier for the vortex to move into the bulk, if x_0 is much higher than the nucleation distance, supposed to be a few times the ξ value. There is some analogy between this surface barrier and the effect of penetration of a vortex into the sample with the edge shape different from rectangular [15].

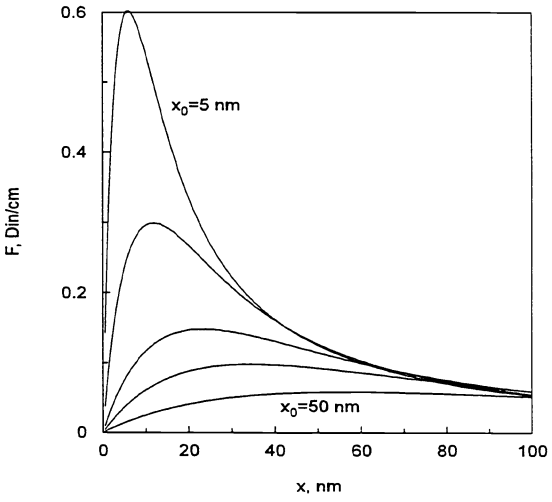

Fig 8. The calculated force acting on a vortex near the surface as a function of the vortex position (x_0=5, 10, 20, 30, 50nm).

Calculation of I-V characteristics of nanobridges was performed following the Aslamazov-Larkin model [16]. Motion of every vortex in the bridge can be described by the equation: $\mathbf{F}=\eta\mathbf{v}$. Here, $\mathbf{F}$ is the sum of forces acting on the vortex due to the vortex-vortex, vortex-transport current and vortex-superconductor edge interaction, η is the viscosity coefficient and $\mathbf{v}$ is the vortex velocity. Since our bridges are quite long, switching of vortices motion from the single path to the multiple path is expected and coincides with the observed features in the experimental I-V characteristics [6]. In Fig.9 the experimental I-V curve of the nanobridge with l=150nm, w=200nm (a), the simulated I-V characteristics assuming standard vortex to surface interaction (b) and calculation using the discussed above edge pinning barrier with superconductor surface degradation (c) is plotted. The parameters used for calculation are: λ_0=140nm, x_0=10nm, $\eta=10^{-7}$ g/cm·sec, the distance of the vortex nucleation from the edge a=2nm. One can see that the latter case fits the experimental curve in a better way. The transition from the superconducting state, with no vortices inside the bridge, to the vortices flow state as well as the switching between multiple paths is much smoother, which fits to the experimental data even at low temperature. The calculated value of $\eta=10^{-7}$ g/cm·sec is one order of magnitude higher than the one estimated earlier [6], which coincides with the Bardeen-Stephen model [14].

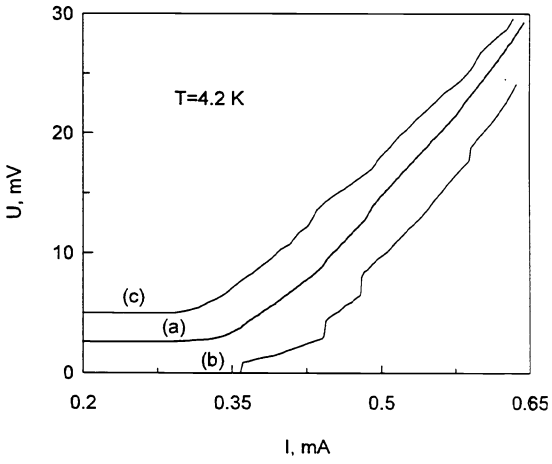

Fig.9 The experimental (a) and calculated (b), (c) I-V characteristics of the 200nm wide bridge at T=4.2K (Curves are shifted along the vertical axis).

The critical current I_c was measured as a function of w. In Fig.10 the experimental values of $I_c(w)$ at T=77.4K are given. Two regions can be distinguished with a crossover point at w≈400nm. This behaviour can be understood assuming that for narrower bridges (w<400nm) the critical current is determined by vortex edge pinning. For wider bridges at the same average current density J_c ($J_c \equiv I_c/A$,

where A is the bridge cross-section area), vortices start to penetrate into the bridge due to the demagnetization effect, and bulk pinning becomes dominant. Finally, the J_c of a bridge goes to a constant value ($J_c=10^6$ A/cm^2 at 77K), which is determined by the material properties.

5. SUMMARY

Nanobridges and SQUIDs based on $YBa_2Cu_3O_7$ thin films have been structured. The unusual temperature dependence of the voltage-flux modulation can be explained by considering degradation of superconductor in the nanobridge area. This leads to a local suppression of T_c and to a transition from SNS to SS'S type junction with decreasing temperature. The exponential spatial distribution of the superconducting parameters in this region was taken. The shape of the surface barrier for a vortex to enter the superconductor was calculated. Using this barrier, the I-V characteristics of superconducting nanobridges were calculated and are in a good agreement with the experimental curves. The experimental $I_c(w)$ dependence of the nanobridge shows the crossover at $w\approx400$nm which can be interpreted as the transition from the dominating role of vortex surface pinning for narrower nanobridges to bulk pinning.

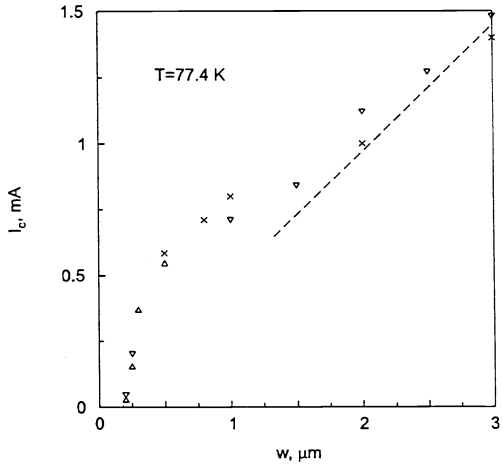

Fig.10 The critical current I_c as a function of nanobridge width w at T=77.4K.

6. REFERENCES

1. A.T.Golovashkin and A.N.Lykov. "Investigation of bridge junctions made of high-temperature superconductor Nb_3Sn," Zh. Aksp. Teor. Fiz., vol. **74**, p.214, 1978; Sov. Phys.-JETP, vol. **47**, pp.110-115, January 1978.
2. K.K.Likharev, "Vortex motion and the Josephson effect in superconducting thin bridges," Zh. Eksp. Teor. Fiz., vol. **61**, pp.1700-1711, October 1971; Sov. Phys.-JETP, vol. **34**, pp.906-912, April 1972.
3. K.K.Likharev, "Superconducting weak links," Review of Morden Physics, vol. **51**, pp.101-159, January 1979.
4. A.H.Dayem and J.J.Wiegand, "Behavior of thin-film superconducting bridges in a microwave field," Phys. Rev., vol. **155** (2), pp.419-429, March 1967.
5. H.Rogalla, *High T_c Josephson contacts. Preparation and properties*, (Habilitation thesis, University of Gissen, Germany, 1986)
6. M.V.Pedyash, G.J.Gerritsma, D.H.A.Blank and H.Rogalla, "Coherent Vortex Motion in Superconducting Nanobridges Based on YBaCuO Thin Films," IEEE Trans. on Appl Sc., vol. **5** (2), p.1387, 1995.
7. D.H.A.Blank, W.Booij, H.Hilgenkamp, B. Vulink, D. Veldhuis, H. Rogalla, "YBCO nanobridge junctions and dc-SQUIDs made by Focused Ion Beam Milling," IEEE Trans. on Appl Sc., vol. **5** (2), p.2786, 1995.
8. D.H.A.Blank, D.J. Adelerhof, J.Flokstra and H.Rogalla, "Preparation of YBaCuO thin films on various substrates by laser ablation," Physica C, vol.**167**, pp.423-432, 1990.
9. S.S.Tinchev, "High-T_c SQUIDs with local oxygen-ion irradiated weak links," IEEE Trans. on Appl. Sc., vol. **3** (1), pp.28-32, March 1993.
10. J.D.Jorsonsen, B.W.Veal, A.P.Paulikas, L.J.Nowicki, G.W.Crabtree, H.Claus and W.K.Kwok, "Structural properties of oxygen-deficient YBaCuO," Phys. Rev. B, vol. **41** (4), pp.1863-1877, February 1990.
11. M.Yu.Kupriyanov, K.K.Likharev and V.F.Lukichev, "Influence of effective electron interaction on the critical current of Josephson weak links," Zh. Aksp. Teor. Fiz., vol. **83**, pp.431-441, July 1982; Sov.Phys.-JETP, vol **56** (1), pp.235-240, July1982.
12. K.Enpuku, Y.Shimomura and T.Kisu, "Effect of thermal noise on the characteristics of a high T_c superconducting quantum interference device," J. Appl. Phys., vol **37** (11), pp.7929-7934, June 1993.
13. M.V.Pedyash, D.H.A. Blank and H. Rogalla, "DC SQUIDs based on YBaCuO nanobridges," accepted for publication in Apll. Phys. Lett., 19 February 1996.
14. Tinkham, *Introduction to Superconductivity* (McGraw-Hill, New York, 1975).
15. R.P.Huebener, R.T.Kampwirth, and J.R.Clem, J. Low. Temp. Phys., Vol. **6**, p.275, 1972.
16. L.G.Aslamazov and A.I. Larkin, "Josephson effect in wide superconducting bridges," Zh. Eksp. Teor. Fiz., vol. **68**, pp.766-775, February 1975; Sov. Phys.-JETP, vol. **41**, pp.381-396, 1975.